


Article

A Compact, Reliable and Efficient 16 Channel Power Supply for the Automated Screening of Semiconducting Metal Oxide Gas Sensors

Christof Hammer ^{1,*}, Johannes Warmer ¹, Sebastian Sporrer ¹, Peter Kaul ¹, Ronald Thoelen ² 
and Norbert Jung ¹

¹ Institute of Safety and Security Research ISF, University of Applied Sciences Bonn-Rhein-Sieg, Grantham-Allee 20, 53757 Sankt Augustin, Germany

² Institute for Materials Research, Hasselt University, Wetenschapspark 1, B-3590 Diepenbeek, Belgium

* Correspondence: christof.hammer@h-brs.de; Tel.: +49-2241-865-289

Received: 10 July 2019; Accepted: 3 August 2019; Published: 9 August 2019



Abstract: The choice of suitable semiconducting metal oxide (MOX) gas sensors for the detection of a specific gas or gas mixture is time-consuming since the sensor's sensitivity needs to be characterized at multiple temperatures to find its optimal operating conditions. To obtain reliable measurement results, it is very important that the power for the sensor's integrated heater is stable, regulated and error-free (or error-tolerant). Especially the error-free requirement can be only be achieved if the power supply implements failure-avoiding and failure-detection methods. The biggest challenge is deriving multiple different voltages from a common supply in an efficient way while keeping the system as small and lightweight as possible. This work presents a reliable, compact, embedded system that addresses the power supply requirements for fully automated simultaneous sensor characterization for up to 16 sensors at multiple temperatures. The system implements efficient (avg. 83.3% efficiency) voltage conversion with low ripple output (<32 mV) and supports static or temperature-cycled heating modes. Voltage and current of each channel are constantly monitored and regulated to guarantee reliable operation. To evaluate the proposed design, 16 sensors were screened. The results are shown in the experimental part of this work.

Keywords: multi-channel power sourcing; semiconducting metal oxide gas sensor array; automated sensor-screening; high degree of diagnostic coverage and reliability

1. Introduction

Metal oxide (MOX) semiconducting gas sensors are used in many different applications such as air quality monitoring [1] or fire detectors [2] because of their low cost and good sensitivity. However, their use also introduces unpleasant shortcomings such as cross-sensitivity, drift or aging [3–6]. A suitable method to manage these unwanted effects is the use of several (different) sensors in an array. This can accommodate for higher selectivity, fault tolerance and error detection. The selectivity can be further increased by operating the entire array, or parts of it, at different static temperatures or in temperature-cycled operation (TCO) [7].

The most important task when designing a gas sensor array is the selection of adequate sensors. This is known as sensor-screening [8–10]. Screening is necessary to find the sensor's optimal operating temperature(s), since the sensitivity of a sensor to a specific gas is strongly dependent on its temperature [11,12]. Another important use for a detailed screening is the characterization of newly developed custom sensor substrates. The screening process and array operation both require a stable, reliable supply to independently power the heater elements of multiple sensors. It has to

support different operating modes per sensor (constant temperature, temperature-cycled operation) and has to have a sufficiently high level of automation. The reliability refers to the ability of the system to detect and handle failure of the power supplied to the attached heater. For later analysis and immediate error reporting, the diagnostic coverage of the system needs to be high. Having such a detailed monitoring capability can, for example, prevent the wasting of measurement time (because of faulty heater behavior) during a long screening process. To accommodate for mobile applications, the power supply has to provide the voltages very efficiently to maximize operating time and minimize power dissipation, eliminating the need for cooling equipment, which would have a negative impact on the systems size and weight. Having a small and compact system is especially interesting if large setups with many sensors are used because it not only reduces the amount of used space, but also helps to increase the structural clarity of such complex setups.

We present a compact and lightweight embedded system that provides 16 individually programmable, fully regulated, supervised power channels which are derived from a common power source. Every channel can be operated in either constant temperature mode or temperature-cycled mode. The voltage conversion is implemented efficiently with low output ripple. The efficiency becomes very interesting if a mobile application is foreseen. All vital parameters are monitored and logged for later analysis. An easy-to-use digital control interface offers a high degree of automation and allows fast and seamless integration of the system into existing measurement setups. Although the screening process for a single sensor cannot be accelerated, this highly automated system enables the screening to be parallelized by evaluating the characteristics of up to 16 sensors simultaneously.

2. Related Work

Considering that this work's main contribution is in the field of powering and monitoring the heater element of MOX gas sensors, we investigated the approaches that have been used and proposed by other research teams for this task. Cardinali et al. [13] proposed an on-off controlled loop, in which the heater is turned on if the heater resistance is higher compared to a target resistance and turned off when the heater resistance is lower. On-off controlled loops can also be combined with both a Wheatstone bridge, where one of the branches is the heater resistance, as well as with a window comparator, like Malfatti et al. showed in 2006 [14]. Amos and Segee implemented the described on-off control loop using a microcontroller [15]. The temperature is adjusted through a power transistor, driven by an unfiltered pulse-width modulated (PWM) signal from the controller. The microcontroller's internal analog-to-digital converter (ADC) reads the voltage drop over the heater to perform a proportional-integral-derivative (PID [16]) controlled adjustment of the PWM signal to stabilize the temperature.

In contrast to switching solutions, the temperature can also be regulated with a proportional direct current. Hansford et al. adjust the heater current with a Wheatstone bridge to feed back an out-of-balance signal proportional to the heater's own resistance [17]. A similar approach is described by Barrettino et al. [18]. They use a transistor driven by an operational amplifier to set the appropriate dc heater current and stabilize it by a feedback signal involving the heater temperature. Unlike Hausford et al., they use a P or PID feedback controller followed by a digital-to-analog converter (DAC) to control the amount of direct current for the heater. The heater temperature is measured by a temperature sensor. In 2014 Somov et al. presented their work on a four-stage heating profile enabled controller [19]. This profile is generated by a microcontroller unit, using the onboard DAC and buffered by an amplifier chip.

In TCO mode the heater-power regulation leads to an alternating modulated temperature profile on the heater. The gas-sensing process and the resulting change in sensor resistance is used to modulate the frequency of this signal. Martinelli et al. propose this kind of regulation based on a multivibrator and a counter [20]. The vibrator frequency follows the heater resistance. This signal drives a simple counter and the carry bit is used to control a voltage-level translator, effectively slowing down the frequency of the vibrator. The output of the voltage translator is used as a feedback signal to control the

heater temperature, thus controlling the frequency of an on-off regulator to modulate the temperature. The frequency of this feedback signal is later used to distinguish between different gases.

Sudarmaji and Kitagawa came up with a very similar design, but use a programmable system-on-a-chip (SoC) to modulate the temperature signal by pulse-width [21]. The work of Schultealbert et al. is featured in a SniffChecker module from 3S GmbH to drive the heater of a tin dioxide (SnO_2) sensor [22]. This tool provides programmable temperature cycles to enable temperature-cycled operation.

This goal of this work is to combine the advantages of all these approaches into a single embedded system that enables a stable DC-controlled temperature regulation for multiple individually programmable channels. In addition to stable setpoints, modulation of temperature cycles is one of the main features demanded for this system, along with minimizing the power dissipation and size.

3. System Design

We propose a small and lightweight embedded system that offers 16 individually programmable, supervised power channels.

The system is designed in a modular fashion and consists of two building blocks, which are depicted in Figure 1. The modularity pays respect to the divide-and-conquer design methodology, offering the highest degree of flexibility, extensibility and maintainability. Figure 1 also shows the prototype of the proposed system fitted with 16 power modules. It is attached to the measuring chamber, which is fitted with the 16 sensors.

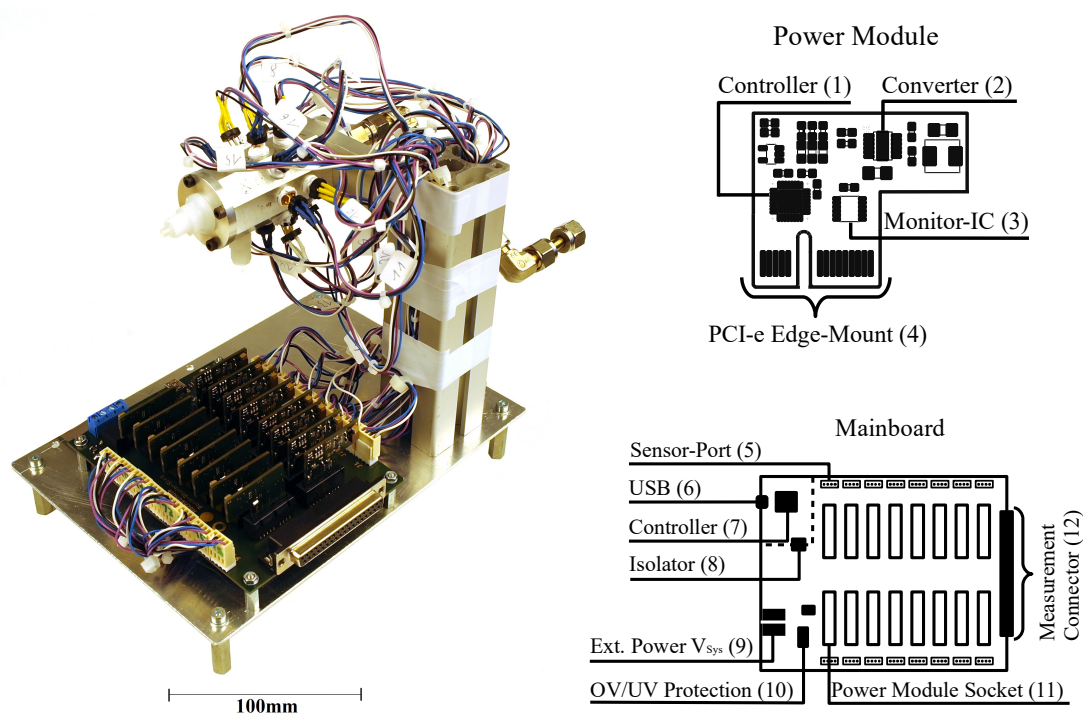


Figure 1. Schematic of the system, depicting a single power module, the mainboard and the prototype connected to 16 sensors, mounted in a measurement chamber.

3.1. Mainboard

The mainboard coordinates the internal and external communication, provides 16 sockets (Figure 1-11) for the power modules and distributes the common system voltage V_{SYS} (Figure 1-9). The MOX gas sensors are connected to 16 sensor ports (Figure 1-5), realized using conventional pin headers. They provide the output of a power channel to the heater on pins 1 & 2 while the

remaining two pins are used to route the sensor signal to the measurement connector (Figure 1-12), to which external measurement equipment (e.g., multimeter) can be connected.

The board is equipped with an STM32F410 series microcontroller [23] (Figure 1-7). Its main task is to relay data from the controlling host (i.e., PC) to the system's internal I²C [24] bus and vice versa, which is realized by a simple control protocol. The latter also allows easy integration of the system into existing measurement setups. The controller circuit is electrically isolated from the power part via bidirectional insulator chips [25] (Figure 1-8), which prevent damage to the host in the event of a critical error on the power side. Since the microcontroller draws its power from the USB bus (Figure 1-6), it will not shut down in case of failure on the power side and will still be able to perform error reporting to the user. For stable unsupervised operation over long time periods, high diagnostic coverage is needed. Therefore, all voltages and currents in the system must be constantly monitored. The following protection circuits and supervision (Figure 1-10) features are implemented: V_{SYS} is protected against undervoltage and overvoltage ($5\text{ V} < V_{SYS} < 12\text{ V}$) as well as reverse voltage conditions down to -40 V . These protections are realized using the circuit depicted in Figure 2.

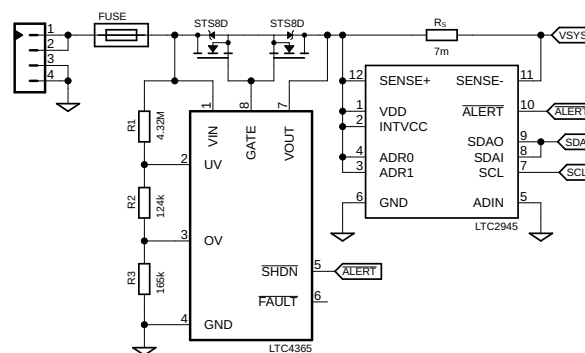


Figure 2. Schematic of the system's overvoltage (OV)/undervoltage (UV) protection from Figure 1.

The supply protection chip LTC4365 [26] controls two external power MOSFETs to ensure that V_{SYS} stays within the user-defined safe operating range. The thresholds for overvoltage (OV) and undervoltage (UV) are set by three external resistors (R_1, R_2, R_3) shown in Figure 2. Overcurrent protection ($I_{SYS} > 16\text{ A}$ for more than 1 ms) is achieved by a replaceable fuse. The continuous supervision of V_{SYS} and I_{SYS} is realized by the LTC2945 [27] power monitor, which measures current with an external shunt resistor R_S and voltage up to 80 V. The measured values are digitized by an internal 12-bit ADC and can be read out via the chip's I²C interface. The shunt value has to be selected so that the voltage drop over the shunt resistor at maximum system current ($I_{SYS_{max}}$) is smaller than $V_{ADC_{max}} = 102.4\text{ mV}$. The shunt value in the design is selected according to the maximum expected current: $16 \times I_{OUT_{max}} + I_{SYS} = 16 \times 0.75\text{ A} + 0.2\text{ A} = 12.2\text{ A}$. Therefore, $R_S < \frac{102.4\text{ mV}}{12.2\text{ A}} \approx 8.4\text{ m}\Omega$ and is implemented as a 7 m Ω resistor using a Kelvin connection with very short trace length (<2 mm). The chip features programmable upper and lower limits for current, voltage and power and emits an alert signal if one of these limits is exceeded. Because the \overline{ALERT} pin of the LTC2945 is connected to the \overline{SHDN} pin of the LTC4365, main power can be automatically switched off without microcontroller interaction. This allows the user to add dynamic programmable current and voltage limits within the resistor-defined hard limits of the LTC4365.

3.2. Power Module

A power module implements the functionality for a single power channel and consists of three main components along with their respective circuit components. To be able to power most commercial sensors, the minimal voltage range for each channel has to be 0 V to 7 V with 50 mV resolution and must be capable of sourcing up to 0.75 A of current (max. 5.25 W total power). The modules are connected to the mainboard by PCIe edge mount connectors (Figure 1-4).

Although unfiltered PWM is the easiest step-down solution, voltage spikes introduced by rapid switching can cause heavy crosstalk between the sensitive layer and integrated heater element.

A typical commercial MOX gas sensor with its layer is shown in Figure 3. Crosstalk is problematic with sensors in which the isolation layer forms a capacitive coupling between the heater and the interdigital structure. Such interference was observed during previous work with certain commercial thin film sensors and is depicted in Figure 4. It shows the crosstalk of an unfiltered 65 kHz PWM signal directly applied to an MLK-type sensor [28]. To avoid such problems, a very low output ripple is required.

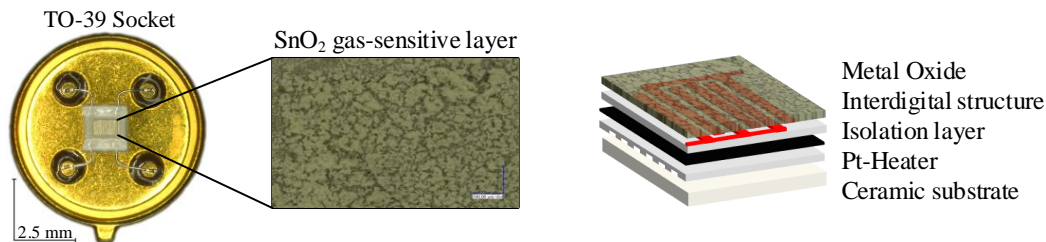


Figure 3. Typical metal oxide (MOX) gas sensor mounted on a TO-39 socket with an enlarged view of its sensitive layer and a schematic representation of its internal structure.

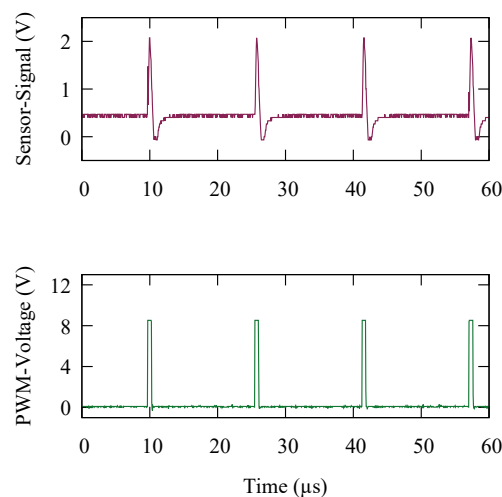


Figure 4. Crosstalk introduced by unfiltered pulse-width modulated (PWM) with 65 kHz base frequency on a commercial thin film MOX gas sensor in air at 2.3 V root mean square voltage applied to the heater element.

Although the use of a low-dropout regulator (LDO) would solve the crosstalk problem, it is a very inefficient way for voltage down conversion because the dropout voltage is simply dissipated as heat. This is especially problematic when the input voltage is much larger than the required output. In this case the overall efficiency will be very low and large heat sinks are necessary to spread the heat, which would unnecessarily increase the system's size and weight.

Therefore, a switching step-down solution with adequate filtering is the best solution for a small and efficient system. In order to obtain a low output ripple while keeping the filter components small, a high switching frequency is required. To obtain the highest possible degree of automation, the output of the step-down regulator has to be programmable.

Consequently, the proposed design is based on a step-down converter for efficient voltage down conversion and a remaining low output ripple with small filter components. Combined with the previously mentioned power supervisor LTC2945, the module is able to provide an active output

regulation and high diagnostic coverage. Both chips are coordinated by a central microcontroller. The internal workings and dependencies of the module are described in the following section.

This design uses the LTC3600 [29] (Figure 1-2), a single-resistor-programmable step-down regulator, with an output range from 0 V to 15 V at up to 1.5 A. The switching frequency of up to 4 MHz allows the use of small filter components. In regular operating mode, the I_{set} pin of the IC provides a current of 50 μA which, in combination with a user selectable resistor, is used to program the desired output voltage. The circuit proposed in this work is depicted in Figure 5. It modifies the regular operating circuit by replacing the resistor with a programmable voltage provided by a DAC. Using this technique, the output of the LTC3600 can now be digitally controlled by a microcontroller.

To obtain a small output ripple while maintaining good efficiency, the output filter components are calculated as follows: because efficiency is higher at low switching frequencies and small ripple current, the LTC3600 is set to 1 MHz. A 47 μF ceramic capacitor with approximately 50 m Ω equivalent series resistance (ESR) was selected as the output capacitor C_{OUT} . Using Equation (1), which is derived from equations found in the applications information chapter of the LTC3600 datasheet [29], the highest allowed ripple current $\Delta I_{L_{MAX}}$ for the chosen capacitor and switching frequency can be calculated.

$$\Delta I_{L_{Max}} \approx \frac{\Delta V_{OUT_{Max}} \cdot 8 \cdot f_{SW} \cdot C_{OUT}}{1 + R_{ESR} \cdot 8 \cdot f_{SW} \cdot C_{OUT}} \quad (1)$$

Using the above specified values, the equation yields $\Delta I_{L_{Max}} = 0.95$ A. This can be used in Equation (2) to calculate the required coil size.

$$L > \frac{V_{OUT}}{f_{SW} \cdot \Delta I_{L_{Max}}} \cdot 1 - \frac{V_{OUT}}{V_{IN_{Max}}} \quad (2)$$

Since Equation (2) yields its maximum at $V_{Out} = \frac{V_{IN_{MAX}}}{2}$, this point specifies the minimal coil value which guarantees a ripple smaller than 50 mV for all values of V_{Out} . With a maximum input voltage of $V_{IN} = 12$ V the minimal coil value is 3.16 μH . Following the recommendations from the LTC3600 datasheet, a 4.7 μH coil of type IHLP2020BZ [30] was chosen.

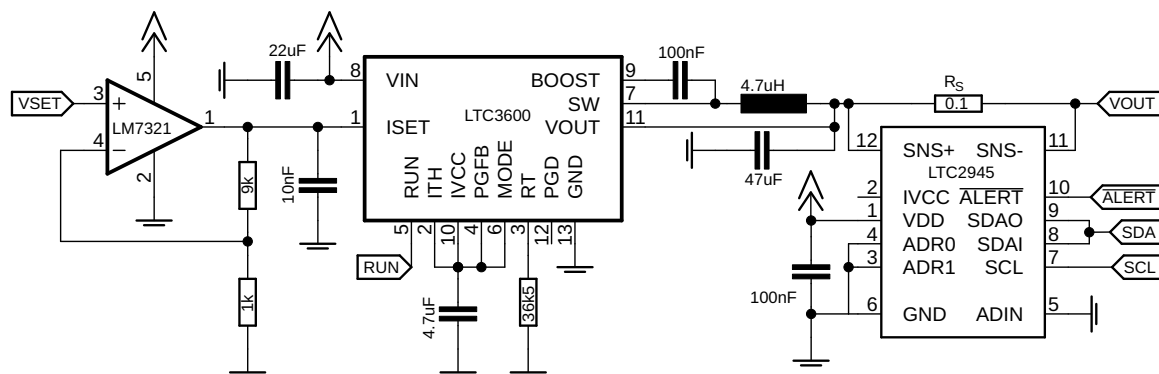


Figure 5. Schematic of the power module, depicting the LTC3600 step-down converter with the LTC2945 power monitor and the LM7321 operational amplifier. The microcontroller is omitted for clarity.

The LTC3600 is combined with a microcontroller (Figure 1-1), which can be programmed to perform supervision, active regulation of the output and support of different operating modes such as TCO, constant current mode, constant voltage mode or user-defined ramp mode. Furthermore, the use of a microcontroller offers the best flexibility in terms of automation.

The main tasks of the controller are, as mentioned above, the supervision and regulation of the output and communication with the mainboard via I²C. To provide the SET voltage of up to 7 V for the LTC3600 with a resolution of 50 mV, a DAC with at least 8-bit resolution is needed. The chosen

STM32L431 [31] offers two 12-bit DACs and two dedicated I²C interfaces in a small 5 mm × 5 mm package with 32 pins. The DAC is used to convert a 12-bit digital value (0–4095) to a proportional analog output voltage (0–2.5 V) which is buffered and amplified by a factor of 6 with an external operational amplifier (LM7321) [32] in non-inverting mode. This voltage is then routed to the VSET pin of the LTC3600. In this configuration, VSET can be as high as 15 V with a resolution of 3.67 mV. Communication with the mainboard is realized by one of the controller's I²C interface which is connected to the system's internal I²C bus. Its bus-address is obtained by four general purpose I/O pins which serve as address configuration pins. The address is hardcoded by the socket on the mainboard.

The output voltage and current from the step-down converter are continuously supervised by the aforementioned power monitor LTC2945 (Figure 1-3). The chip and the microcontroller form a closed control loop allowing for either current or voltage to be regulated to a user-selectable target value. The shunt value of 0.1 Ω has been selected to measure a current of up to 1.0 A. The chip's upper and lower boundaries for current and voltage are automatically set by the microcontroller depending on the user-selected target value. If a parameter is over the limit the LTC2945's $\overline{\text{Alert}}$ pin is pulled low, generating an interrupt on the microcontroller, which shuts down the LTC3600 by pulling its RUN pin low. Then, the LTC2945's error register is read and the contained information about what kind of error occurred is relayed to the system's operator as human readable error. Figure 5 shows the connection of the LTC3600 to the power supervisor LTC2945 and DAC amplifier.

3.3. Firmware

The firmware of the power modules implements the before mentioned operating modes, active output regulation and configures the dynamic protection limits for the power monitor.

The regulation is realized with a standard PID regulation algorithm. Current and voltage output from the LTC3600 are obtained from the LTC2945 with a sampling frequency of 5 Hz (maximum sampling speed of the LTC2945). An adjusted VSET value is calculated by the PID algorithm according to the reference value (set by the user), the read back value and the regulation parameters for the proportional, integral and differential parts (K_p , K_i and K_d). The experimentally chosen regulation parameters for K_p , K_i and K_d are optimized to prevent voltage overshoots at the cost of a longer rise time. The values can however easily be modified by the user if required. The PID regulation is available in all modes and can be disabled if needed.

The actual heater temperature can only be regulated indirectly as a function of the heater element's resistance and material-specific parameters which are provided by most sensor manufacturers. If the heater material parameters are known, the firmware calculates the actual temperature of the heater and logs it as an additional parameter alongside voltage and current. Currently, this functionality is only implemented for sensor types of the manufacturer UST (Umweltsensorik GmbH, Germany) [33] but can be easily extended to other sensor types.

A non-volatile, programmable user page located in the microcontroller's memory can hold sensor-specific information (like recommended and maximum heater voltage, sensor production date etc.) as well as board specific data e.g., the before mentioned parameters for the PID regulation.

3.4. Communication Protocol

The system is controlled by an easy-to-use byte-sequence protocol over a virtual serial port provided via USB. This option provides the simplest way to integrate the system into existing software solutions (e.g., LabView) and is natively supported by many operating systems. The structure of the protocol is shown in Table 1. Instructions to the system and the responses from the system are transmitted as a sequence of bytes. Such byte-sequences are also known as a packet. Each packet has a fixed number of bytes which is determined by the command.

Every command starts with a fixed start byte followed by the address of the target. The protocol supports individual addressing as well as broadcasts. The address is followed by the command itself and an optional command-specific payload (e.g., voltage in mV). After the payload, a fixed trailer sequence indicates the end of a packet. To make the protocol more robust against random transmission errors, the user can enable a 32-bit cyclic redundancy check (CRC). The CRC32 algorithm computes a checksum over the data bytes. The additional bytes are added between the payload and the termination sequence.

All functions of the system can be controlled using the protocol. For standalone testing a simple graphical user interface that generates the required byte sequences and interprets the system's response has been implemented.

Table 1. Structure of the communication protocol.

	Head	I ² C Address	Command	Data	CRC	Trail
Bytes	1	1	1	0:10	4	3
Value	0 × F0	0 × 00:0 × 0F	Variable	Variable	Variable	0 × FF 0 × 0D 0 × 0A

4. System Validation

In order to evaluate the functionality and efficiency of the developed system, a single channel of the system was tested against reference implementations of the most common heater power circuits: an adjustable low-dropout regulator (TS317) in a standard application circuit ([34] p. 1), an emitter follower circuit ([35] p. 899) with a Darlington pair transistor (D209L) and a high-power operational amplifier (OPA548F) in non-inverting configuration as described in ([35] p. 496).

The output voltage was increased in steps of 0.1 V up to the maximum achievable output for each respective circuit. Input and output voltages and currents were measured on all circuits and the conversion efficiency calculated according to: $\eta = \frac{P_{Out}}{P_{In}} = \frac{V_{Out} \cdot I_{Out}}{V_{In} \cdot I_{In}} \cdot 100\%$.

Since most commercial sensors employ heater elements in the range from 10 Ω to 100 Ω , a load resistor $R_L = 10 \Omega$ with a power rating of 20 W acts as a suitable replacement in all test circuits. Furthermore, choosing a small resistive value (i.e., bigger load) helps to evaluate the system under more demanding conditions. The results from the efficiency measurements of all evaluated circuits are combined in Figure 6.

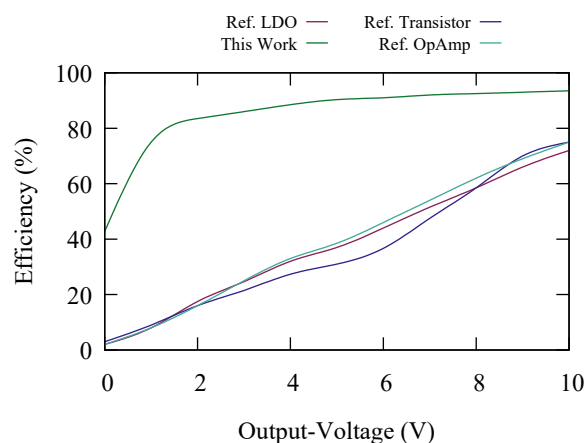


Figure 6. Measured efficiency of the evaluated circuits.

The output ripple of the system and the reference circuits was also measured during the efficiency tests. The results are depicted in Figure 7. The measured ripple never surpassed 32 mV.

In addition to the efficiency measurements, the temperature of each circuit was monitored with a thermal-imaging camera (optris PI 400). Figure 8 shows an exemplary thermal image of a single power module of the developed system supplying 10 V to the load resistor. The dropout-regulator, voltage-follower and operational-amplifier circuits quickly reached the point of thermal shutdown (~ 2 V, see Figure 9) and therefore required large external heat sinks in order to function correctly at higher output voltages. All measurements were performed with heat sinks attached to the components. Figure 9 summarizes the results of all temperature measurements and clearly shows that the step-down converter exhibits considerably lower heat dissipation compared to the non-switching alternatives.

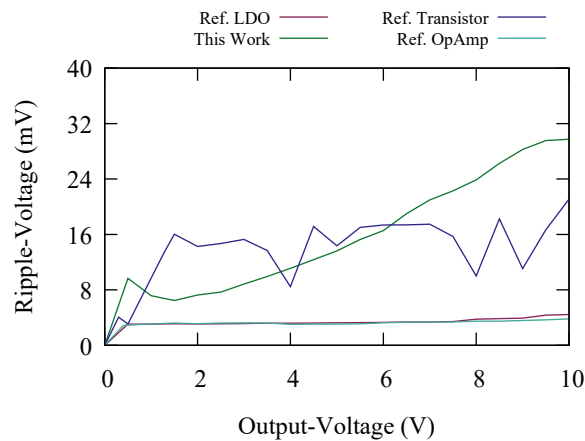


Figure 7. Measured output ripple of a power module with 10 Ω load resistor in the voltage range from 0.5 V to 12 V.

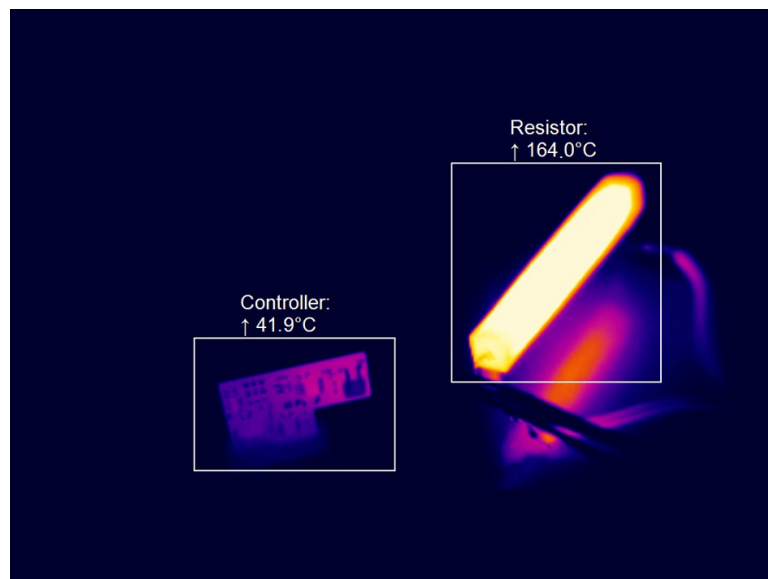


Figure 8. Thermal image of a single power module with 10 Ω load resistor at 10 V output voltage.

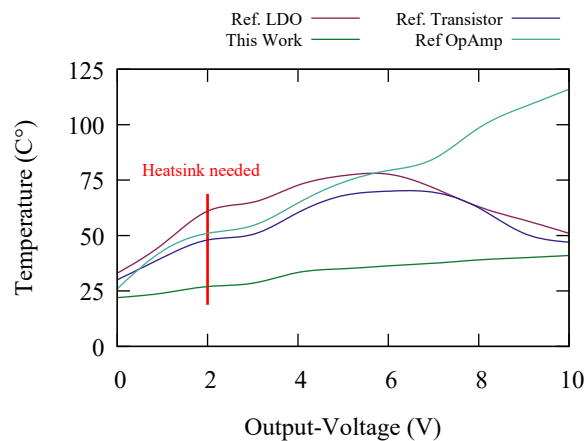


Figure 9. Temperature comparison of the evaluated circuits.

A special set of tests was dedicated to the evaluation of the diagnostic coverage. For these tests the output of the step-down converter was short-circuited in order to create an over-current alert. The main power lines were then also short-circuited in order to test the fuse as well as the error reporting performed by the mainboard's microcontroller. Failure or misbehavior of single power modules were also simulated by manipulating firmware parameters (e.g., by overriding the target output voltage without adjusting the protection limits) with an external debugger. All the performed tests were completed successfully and the system always behaved as intended by design.

After the completion of the application example (216 h) for this work, the prototypical system was in use for about 6 more months in different measurement applications. During this time the system performed without errors.

5. Application Example

In order to test the system in the previously mentioned screening process, it was integrated into an existing gas-mixing unit (GMU) and a basic parallel sensor screening was performed on 15 custom-built metal oxide semiconductor gas sensors.

For the evaluation a GMU consisting of five mass flow controllers (MFC) (Model 1179C MKS Instruments Deutschland GmbH, Munich, Germany) as depicted in Figure 10 was used. A flow of synthetic air (20.5 % O₂, rest N₂, hydrocarbon-free, Westfalen AG, Münster, Germany) can be controlled up to 1000 sccm (MFC 1) while the humidity can be adjusted by bubbling the synthetic air through two flasks filled with water (MFC 2). The remaining three MFCs (MFC 3–5 max. flow 20 sccm) are connected to the test gases. For the evaluation, carbon monoxide (500 ppm in synthetic air, Westfalen AG, Münster, Germany), nitrogen dioxide (1000 ppm in synthetic air, Westfalen AG, Münster, Germany) and acetone (500 ppm in synthetic air, Westfalen AG, Münster, Germany) were chosen as typical representatives of volatile organic compounds (VOC). The individual sensor resistances were measured using a Keithley model 2700 multimeter equipped with 20-channel differential multiplexer module type 7700 (Keithley Instruments, Cleveland, Ohio, US).

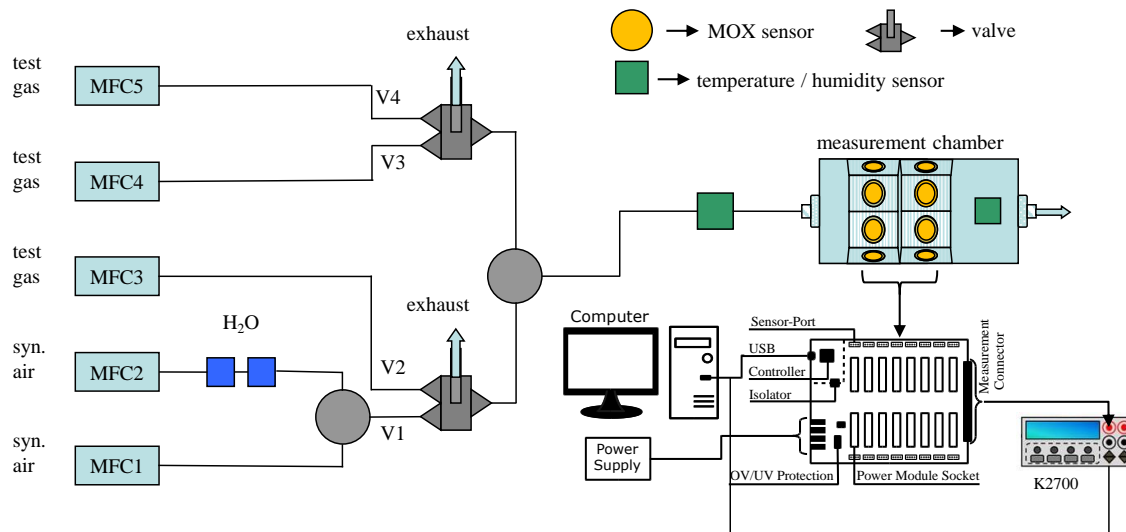


Figure 10. Scheme of the gas mixing unit connected to the presented system, measurement equipment and PC. Mass flow controllers (MFC) 1–5 regulate the gas flows and ratios between test gases, synthetic air and humidity for concentration adjustment. The valve system allows the generation of complex gas mixtures for the sensor tests.

A total of 15 custom sensors were manufactured to evaluate the performance of different metal oxides and their reaction to the target gases. Commercially available sensor substrates of type x33x by UST were applied with a simple drop-coating of tin dioxide, tungsten trioxide, zinc oxide, indium oxide and copper (II) oxide. All oxides were procured from Sigma Aldrich, Munich, Germany and are nanopowders < 100 nm. 10 mg of each oxide was mixed with 100 μ L ultra-pure water supported by an ultrasonic bath. 3 μ L of the suspension was drop-coated on the substrate using a pipette. After drying the sensors at room temperature for 24 h, they were heated up to 800 $^{\circ}$ C for 1 h. For each metal oxide three test sensors were produced. A single reference sensor (TGS 2620 Figaro, Osaka, Japan) completes the test set of 16 sensors. The reference sensor is operated at constant temperature (5 V heater voltage) in all experiments.

The 15 custom sensors were varied in the range of 200 $^{\circ}$ C (2.46 V) to 550 $^{\circ}$ C (5.68 V) with an increment of 50 $^{\circ}$ C per step. At each temperature, the sensors were exposed to each test gas for 10 min followed by a recovery time of 1 h, repeating the process three times. After modifying the heater voltage, a settling time of 1 h was given to allow the sensor to reach its new temperature. The sensitivity S was calculated from the raw data as shown in Equation (3). R_0 and R_x represent the mean value of the measured resistance over a time period of 2 min prior to and after analyte exposition at the end of each timestep.

$$S = \frac{R_0 - R_x}{R_0} \quad (3)$$

Figure 11 shows the results of these experiments. For clarity and since some of the used sensors, due to manufacturing tolerances, can exhibit resistances exceeding the measuring range of the used multimeter (120 M Ω), the data from only one sensor per metal oxide is presented in the graphs.

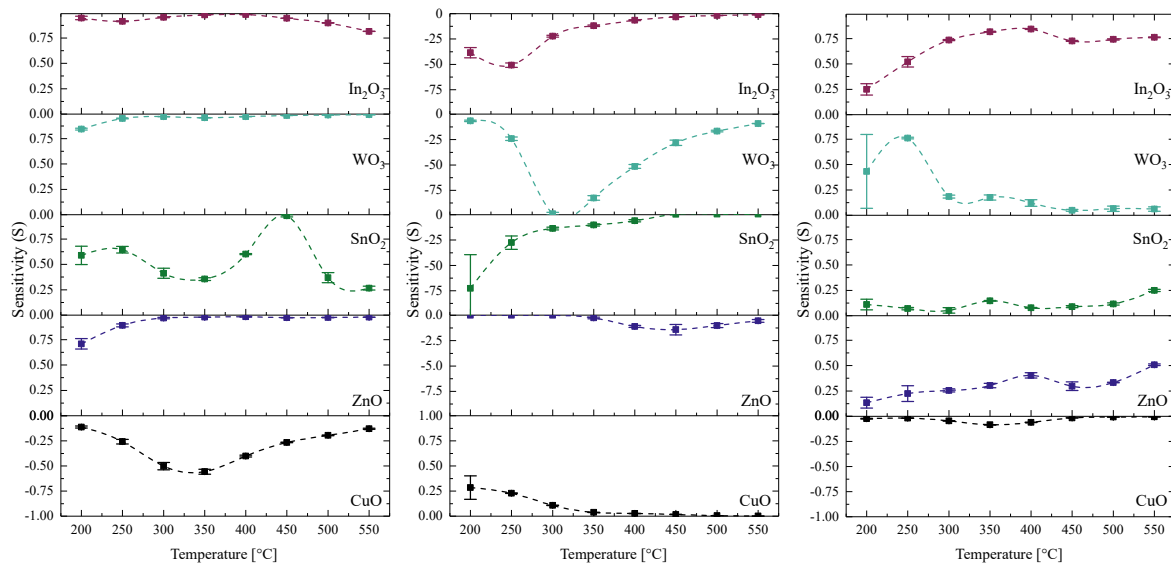


Figure 11. Temperature dependence of the sensor’s sensitivity (S) to (left) acetone (50 ppm), (middle) CO (50 ppm), (right) NO₂ (5 ppm). Relative humidity at 50 %.

The results represent a typical sensor screening experiment. Different metal oxides show different local minima/maxima in their reaction at different temperatures. Based on these results a suitable selection of sensors and their respective parameters could now be chosen to solve the problem of distinguishing between these three substances, for example in fire detectors.

Figure 12 depicts the efficiency of the system with 16 sensors attached and main power set to 12 V. The parabolic shape of the curve is explained by the uneven number of sensors and the measurement program, which powers all odd-numbered (8 modules) sensors in upwards fashion while the even-numbered (7 modules) sensors are powered in the reverse order. Therefore the most power is drawn when all sensors are at the same heater voltage (halfway through the measurement program), in this case the systems averaged output (including the static reference sensor’s 5 V) is 4.13 V. The system maintains an average efficiency of 83.3 %. The highest module temperature observed by thermal imaging camera was 43.9 °C with an average temperature of 37.8 °C.

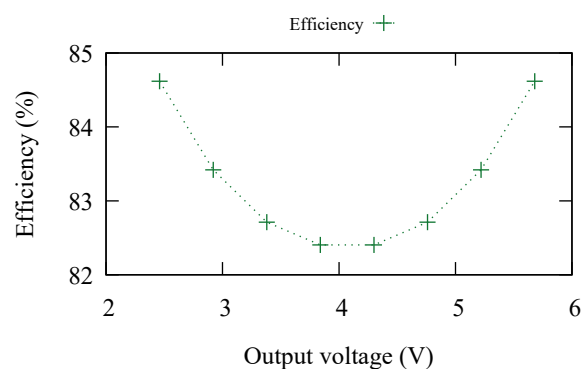


Figure 12. The efficiency of the complete system with 16 sensors attached, measured during the screening experiment. The output voltage is derived as the average over all channels.

6. Conclusions

The average system efficiency measured during the application example from Section 5 was approximately 80 %, which is, compared to the best non-switching solution (power-OP-amp circuit with 30 % efficiency at 4.13 V output voltage), an improvement of 50 %. The measured efficiency can

be further improved, e.g., by taking advantage of currently unused energy saving features of the used microcontrollers and by disabling all active (up to 40) LEDs used for signaling purposes.

The presented system is able to independently power the heater elements of up to 16 MOX gas sensors from a single common power supply. Central protections against overvoltage, undervoltage and overcurrent conditions are implemented. With an output range of 0 V to 15 V with up to 1 A per channel, the system easily satisfies the power requirements of most commercial and custom made MOX sensors. Each channel performs an active PID regulation to obtain a stable output voltage. Regulation parameters can be easily changed by the user if necessary. The remaining ripple voltage on the output is sufficiently low (max. 32 mV) to power thin film sensors without injecting crosstalk between heater element and sensitive layer. All currents and voltages in the system are constantly monitored. As a result, the system attains a high level of diagnostic coverage which is essential for reliability, stability and best possible measurement quality over long periods of time. The use of microcontrollers provides a high level of automation supporting unsupervised long term operation and multiple operation modes. Additional functionality can be implemented by firmware, providing good extensibility. An easy-to-use control protocol and USB interface allow quick integration into existing measurement setups. All aspects of the system can be controlled and supervised using the protocol. The dimensions of the realized system are 100 mm × 100 mm × 35 mm at a weight of 193 g. Its modular structure allows for easy repair and maintenance in case of a hardware failure e.g., by replacing or modifying only a single channel module. No cooling equipment e.g., heat sinks is required. As mentioned above, the system performed without errors over a period of 6 month, which can be seen as a passed long-term test for the systems reliability.

It can be concluded that the system presented in this paper meets all of the requirements to power up to 16 MOX sensors at different voltages and different operating modes, is very stable and efficient over a long period of time and thus provides a highly flexible and versatile platform for future research.

Author Contributions: C.H. is the lead author and was responsible for the system design, hardware construction, software development, efficiency comparison experiments and writing the final paper. J.W. is co-author of this work. He designed and executed the application example presented in Chapter 5. S.S. was tasked with research for the related work and wrote a draft of Chapter 2. P.K. and N.J. are the directors of the Institute of Safety and Security Research (ISF). R.T. and N.J. are the referees in the Ph.D. proceedings of C.H. They all contributed to the work by providing design advice, experimental setup guidance, project coordination and several iterations of paper review.

Funding: This research received internal funding from the Institute of Safety and Security Research at BRS-U.

Conflicts of Interest: The authors declare no conflicts of interest.

References

1. Binions, R.; Naik, A. 13—Metal oxide semiconductor gas sensors in environmental monitoring. In *Semiconductor Gas Sensors*; Jaaniso, R., Tan, O.K., Eds.; Woodhead Publishing Series in Electronic and Optical Materials; Woodhead Publishing: Sawston, UK, 2013; pp. 433–466. [\[CrossRef\]](#)
2. Gutmacher, D.; Foelmli, C.; Vollenweider, W.; Hofer, U.; Wöllenstein, J. Comparison of gas sensor technologies for fire gas detection. *Procedia Eng.* **2011**, *25*, 1121–1124. [\[CrossRef\]](#)
3. Heilig, A.; Bârsan, N.; Weimar, U.; Schweizer-Berberich, M.; Gardner, J.; Göpel, W. Gas identification by modulating temperatures of SnO₂-based thick film sensors. *Sens. Actuators B Chem.* **1997**, *43*, 45–51. [\[CrossRef\]](#)
4. Padilla, M.; Perera, A.; Montoliu, I.; Chaudry, A.; Persaud, K.; Marco, S. Drift compensation of gas sensor array data by Orthogonal Signal Correction. *Chemom. Intell. Lab. Syst.* **2010**, *100*, 28–35. [\[CrossRef\]](#)
5. Lee, A.P.; Reedy, B.J. Temperature modulation in semiconductor gas sensing. *Sens. Actuators B Chem.* **1999**, *60*, 35–42. [\[CrossRef\]](#)
6. Vergara, A.; Lobet, E.; Brezmes, J.; Vilanova, X.; Stankova, M.; Gracia, I.; Cane, C.; Correig, X. Optimized multi-frequency temperature modulation of microhotplate gas sensors. In *Proceedings of the IEEE 2004 SENSORS*, Vienna, Austria, 24–27 October 2004; Volume 3, pp. 1392–1395. [\[CrossRef\]](#)

7. Fonollosa, J.; Fernández, L.; Huerta, R.; Gutiérrez-Gálvez, A.; Marco, S. Temperature optimization of metal oxide sensor arrays using Mutual Information. *Sens. Actuators B Chem.* **2013**, *187*, 331–339. [[CrossRef](#)]
8. Wehrenfennig, C.; Schott, M.; Gasch, T.; Sauerwald, T.; Düring, R.A.; Vilcinskas, A.; Kohl, C.D. Laboratory characterization of metal-oxide sensors intended for in situ analyses of pheromones—SOMMSA approach. *Phys. Status Solidi A* **2012**, *209*, 935–939. [[CrossRef](#)]
9. Zhang, G.; Xie, C.; Zhang, S.; Zhao, J.; Lei, T.; Zeng, D. Temperature-Programmed Technique Accompanied with High-Throughput Methodology for Rapidly Searching the Optimal Operating Temperature of MOX Gas Sensors. *ACS Comb. Sci.* **2014**, *16*, 459–465. [[CrossRef](#)] [[PubMed](#)]
10. Zhang, J.; Qin, Z.; Zeng, D.; Xie, C. Metal-oxide-semiconductor based gas sensors: screening, preparation, and integration. *Phys. Chem. Chem. Phys.* **2017**, *19*, 6313–6329. [[CrossRef](#)] [[PubMed](#)]
11. Yamazoe, N.; Sakai, G.; Shimano, K. Oxide Semiconductor Gas Sensors. *Catal. Surv. Asia* **2003**, *7*, 63–75. [[CrossRef](#)]
12. Wang, C.; Yin, L.; Zhang, L.; Xiang, D.; Gao, R. Metal Oxide Gas Sensors: Sensitivity and Influencing Factors. *Sensors* **2010**, *10*, 2088–2106. [[CrossRef](#)]
13. Cardinali, G.C.; Dori, L.; Fiorini, M.; Sayago, I.; Faglia, G.; Perego, C.; Sberveglieri, G.; Liberali, V.; Maloberti, F.; Tonietto, D. A Smart Sensor System for Carbon Monoxide Detection. *Analog Integr. Circuits Signal Process.* **1997**, *14*, 275–296. [[CrossRef](#)]
14. Malfatti, M.; Stoppa, D.; Simoni, A.; Lorenzelli, L.; Adami, A.; Baschiroto, A. A CMOS Interface for a Gas-Sensor Array with a 0.5 %-Linearity over 500 k/spl Omega/-to-1 G/spl Omega/ Range and 2.5/spl deg/C Temperature Control Accuracy. In Proceedings of the 2006 IEEE International Solid State Circuits Conference—Digest of Technical Papers, San Francisco, CA, USA, 6–9 February 2006; pp. 1131–1140. [[CrossRef](#)]
15. Amos, M.; Segee, B. Micro-controller based Heater Control for Gas Sensors. In Proceedings of the 2001 American Society for Engineering Education Annual Conference & Exposition, Albuquerque, NM, USA, 24–27 June 2001; pp. 6.721.1–6.721.6.
16. PID Theory Explained. Available online: <http://www.webcitation.org/78PZ5UGOP> (accessed on 16 May 2019).
17. Hansford, G.M.; Freshwater, R.A.; Bosch, R.A.; Cox, R.A.; Jones, R.L.; Pratt, K.F.E.; Williams, D.E. A low cost instrument based on a solid state sensor for balloon-borne atmospheric O₃ profile sounding. *J. Environ. Monit.* **2005**, *7*, 158–162. [[CrossRef](#)] [[PubMed](#)]
18. Barrettino, D.; Graf, M.; Taschini, S.; Hafizovic, S.; Hagleitner, C.; Hierlemann, A. CMOS Monolithic Metal-Oxide Gas Sensor Microsystems. *IEEE Sens. J.* **2006**, *6*, 276–286. [[CrossRef](#)]
19. Somov, A.; Baranov, A.; Spirjakin, D.; Passerone, R. Circuit Design and Power Consumption Analysis of Wireless Gas Sensor Nodes: One-Sensor Versus Two-Sensor Approach. *IEEE Sens. J.* **2014**, *14*, 2056–2063. [[CrossRef](#)]
20. Martinelli, E.; Polese, D.; Catini, A.; D’Amico, A.; Natale, C.D. Self-adapted temperature modulation in metal-oxide semiconductor gas sensors. *Sens. Actuators B Chem.* **2012**, *161*, 534–541. [[CrossRef](#)]
21. Sudarmaji, A.; Kitagawa, A. Temperature Modulation with Specified Detection Point on Metal Oxide Semiconductor Gas Sensors for E-Nose Application. *Sens. Transducers* **2015**, *186*, 93–103.
22. Schultealbert, C.; Baur, T.; Schütze, A.; Böttcher, S.; Sauerwald, T. A novel approach towards calibrated measurement of trace gases using metal oxide semiconductor sensors. *Sens. Actuators B Chem.* **2017**, *239*, 390–396. [[CrossRef](#)]
23. STMicroelectronics. *STM32F410x8 Datasheet*; Rev. 6; STMicroelectronics: Amsterdam, Netherlands, 2017 Available online: <https://www.st.com/resource/en/datasheet/stm32f410cb.pdf> (accessed on 5 August 2019).
24. I2C-Bus: What’s that? Available online: <http://www.webcitation.org/78PYumH1g> (accessed on 16 May 2019).
25. Texas Instruments Incorporation. *ISO154x—Low-Power Bidirectional I2C Isolators*, December 2016 ed.; SLLSEB6D; Texas Instruments: Dallas, TX, USA, 2016. Available online: <http://www.ti.com/lit/ds/symlink/iso1540.pdf> (accessed on 5 August 2019).

26. Linear Technology Corporation. *LTC4365—Overvoltage, Undervoltage and Reverse Supply Protection Controller*, September 2013 ed.; Rev. D; Linear Technology Corporation: Milpitas, CA, USA, 2013. Available online: <https://www.analog.com/media/en/technical-documentation/data-sheets/4365fa.pdf> (accessed on 5 August 2019).
27. Linear Technology Corporation. *LTC 2945—Wide Range I2C Power Monitor*, September 2015 ed.; REV. B; Linear Technology Corporation: Milpitas, CA, USA, 2015. Available online: <https://www.analog.com/media/en/technical-documentation/data-sheets/2945fb.pdf> (accessed on 5 August 2019).
28. AppliedSensor. *AS-MLK—Natural Gas Sensor*; AppliedSensor Sweden AB: Linköping, Sweden, 2012.
29. Linear Technology Incorporated. *LTC3600—15 V, 1.5 A Synchronous Rail-to-Rail Single Resistor Step-Down Regulator*, June 2016 ed.; REV. D; Linear Technology Corporation: Milpitas, CA, USA, 2016. Available online: <https://www.analog.com/media/en/technical-documentation/data-sheets/3600fd.pdf> (accessed on 5 August 2019).
30. IHLP Commercial Inductors. *IHLP—High Saturation Coil Series Datasheet*; Rev. 07.07.17; 2017. Available online: <https://www.vishay.com/docs/34253/ihlp-2020bz-01.pdf> (accessed on 5 August 2019).
31. STMicroelectronics. *STM32L431—Ultra-low-power Arm Cortex-M4 32-bit MCU*; DS11451 Rev. 4; 2018. Available online: <https://www.st.com/resource/en/datasheet/stm32l432kc.pdf> (accessed on 5 August 2019).
32. Texas Instruments Incorporation. *LM 7321—Single Ch, RRIO, High Output Current & Unlimited Cap Load +/-15 V Op Amp*, September 2015 ed.; SNOSAW8E; Texas Instruments: Dallas, TX, USA, 2015. Available online: <http://www.ti.com/lit/ds/symlink/lm7322.pdf> (accessed on 5 August 2019).
33. UST Umweltsensortechnik GmbH. *MOX Gas Sensors—Calculation of the Operation Temperature*, March 2016 ed.; 2016. Available online: http://www.umweltsensortechnik.de/fileadmin/assets/downloads/gassensoren/single/TechInfo_MOX-gas-sensors_Calculation_of_the_operating_temperature_Rev1603.pdf (accessed on 5 August 2019).
34. Taiwan Semiconductor Co. Ltd. *TS317—3-Terminal Adjustable Positive Voltage Regulator Datasheet*; Version E15; 2015. Available online: https://www.taiwansemi.com/products/datasheet/TS317_E15.pdf (accessed on 5 August 2019).
35. Tietze, U.; Schenk, C.; Gamm, E. *Halbleiter-Schaltungstechnik*; Springer-Verlag GmbH: Berlin/Heidelberg, Germany, 2012.



© 2019 by the authors. Licensee MDPI, Basel, Switzerland. This article is an open access article distributed under the terms and conditions of the Creative Commons Attribution (CC BY) license (<http://creativecommons.org/licenses/by/4.0/>).